

# Phase behavior and self-assembly of perfectly sequence-defined and monodisperse multiblock copolypeptides

Sarah R. MacEwan,<sup>1,2,†</sup> Isaac Weitzhandler,<sup>1,2</sup> Ingo Hoffman,<sup>3, §</sup> Jan Genzer,<sup>2, 4</sup> Michael Gradzielski,<sup>3</sup> Ashutosh Chilkoti<sup>1,2,\*</sup>

<sup>1</sup> Department of Biomedical Engineering, Duke University, Durham, NC, 27708

<sup>2</sup> Research Triangle Materials Research Science and Engineering Center, Durham, NC, 27708

<sup>3</sup> Stranski-Laboratorium fur Physikalische und Theoretische Chemie, Institut fur Chemie, Technische Universitat Berlin, 10623, Berlin, Germany

<sup>4</sup> Department of Chemical and Biomolecular Engineering, North Carolina State University, Raleigh, NC 27695

<sup>†</sup> Present Address: Institute for Molecular Engineering, University of Chicago, Chicago, IL 60637

<sup>§</sup> Present Address: Institut Laue-Langevin, 71 avenue des Martyrs, 38000 Grenoble, France.

\* Corresponding author: chilkoti@duke.edu

## Supporting Information

**Table S1.** Nomenclature and sequence of block copolymer ELPs.

Abbreviation	Sequence
ELP-S <sub>comp</sub>	G-(SGVPG) <sub>120</sub> -Y
ELP-V <sub>comp</sub>	G-(VGVPNG) <sub>120</sub> -Y
ELP-SVB <sub>1</sub>	G-[SGVPG)-(VGVPNG)] <sub>60</sub> -Y
ELP-SVB <sub>5</sub>	G-[(SGVPG) <sub>5</sub> -(VGVPNG) <sub>5</sub> ] <sub>12</sub> -Y
ELP-SVB <sub>10</sub>	G-[(SGVPG) <sub>10</sub> -(VGVPNG) <sub>10</sub> ] <sub>6</sub> -Y
ELP-SVB <sub>20</sub>	G-[(SGVPG) <sub>20</sub> -(VGVPNG) <sub>20</sub> ] <sub>3</sub> -Y
ELP-SVB <sub>30</sub>	G-[(SGVPG) <sub>30</sub> -(VGVPNG) <sub>30</sub> ] <sub>2</sub> -Y
ELP-SVT <sub>VSV</sub>	G-(VGVPNG) <sub>30</sub> -(SGVPG) <sub>60</sub> -(VGVPNG) <sub>30</sub> -Y
ELP-SVT <sub>SVS</sub>	G-(SGVPG) <sub>30</sub> -(VGVPNG) <sub>60</sub> -(SGVPG) <sub>30</sub> -Y
ELP-SVD <sub>SV</sub>	G-(SGVPG) <sub>60</sub> -(VGVPNG) <sub>60</sub> -Y
ELP-SVG <sub>L</sub>	G-(SGVPG) <sub>30</sub> -(VGVPNG) <sub>5</sub> -(SGVPG) <sub>10</sub> -(VGVPNG) <sub>5</sub> -(SGVPG) <sub>5</sub> -(VGVPNG) <sub>5</sub> -(SGVPG) <sub>5</sub> -(VGVPNG) <sub>5</sub> -(SGVPG) <sub>5</sub> -(VGVPNG) <sub>30</sub> -Y
ELP-SVG <sub>I</sub>	G-(SGVPG) <sub>35</sub> -(VGVPNG) <sub>5</sub> -(SGVPG) <sub>10</sub> -(VGVPNG) <sub>10</sub> -(SGVPG) <sub>10</sub> -(VGVPNG) <sub>10</sub> -(SGVPG) <sub>5</sub> -(VGVPNG) <sub>5</sub> -(VGVPNG) <sub>35</sub> -Y
ELP-SVG <sub>H</sub>	G-(SGVPG) <sub>40</sub> -(VGVPNG) <sub>5</sub> -(SGVPG) <sub>10</sub> -(VGVPNG) <sub>5</sub> -(SGVPG) <sub>5</sub> -(VGVPNG) <sub>10</sub> -(SGVPG) <sub>5</sub> -(VGVPNG) <sub>40</sub> -Y

## A) ELP-S<sub>comp</sub>

## B) ELP-V<sub>comp</sub>

### C) ELP-SVB<sub>1</sub>

D) ELP-SVB<sub>5</sub>

## E) ELP-SVB<sub>10</sub>

## F) ELP-SVB<sub>20</sub>

## G) ELP-SVB<sub>30</sub>

## H) ELP-SVT<sub>y</sub>sv

## I) ELP-SVT<sub>sys</sub>

## J) ELP-SVD<sub>sv</sub>

## K) ELP-SVG<sub>L</sub>

## L) ELP-SVG<sub>I</sub>

## M) ELP-SVG<sub>H</sub>

**Figure S1.** DNA and polypeptide sequences. All ELPs were recombinantly synthesized from short oligomers using concatemerization and recursive directional ligation by plasmid

reconstruction (PRe-RDL).<sup>1</sup> Each ELP gene included a leader composed of a methionine and glycine residue that preceded the ELP sequence. Each ELP gene also included a trailer composed of a tyrosine residue that succeeded the ELP sequence, providing optical activity at 280 nm with an extinction coefficient of  $1280 \text{ M}^{-1}\text{cm}^{-1}$ . Hydrophilic monomers composed of the pentapeptide SGVPG are marked in blue, while hydrophobic monomers composed of the pentapeptide VGVPG are marked in red.

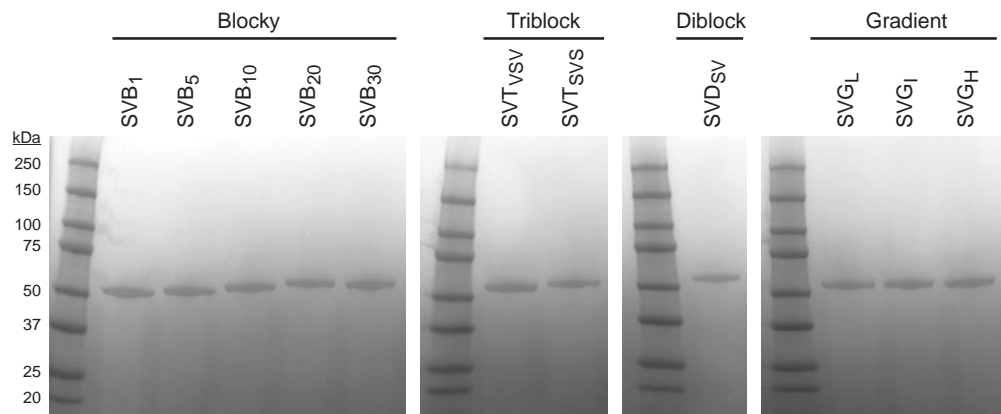


**Figure S2.** Evaluation of purity and size by gel electrophoresis. The purity and size of all ELPs was confirmed with SDS-PAGE and CuCl<sub>2</sub> staining. All ELPs ran slightly higher than their expected MW of 48.66 kDa, which has been reported previously for other ELPs.<sup>2</sup> There were slight variations in the migration of the bands, likely influenced by differences in polypeptide architecture, where trends in migration were apparent within classes of ELPs. For instance, the bands appeared to migrate more slowly in accordance with increasing block size.

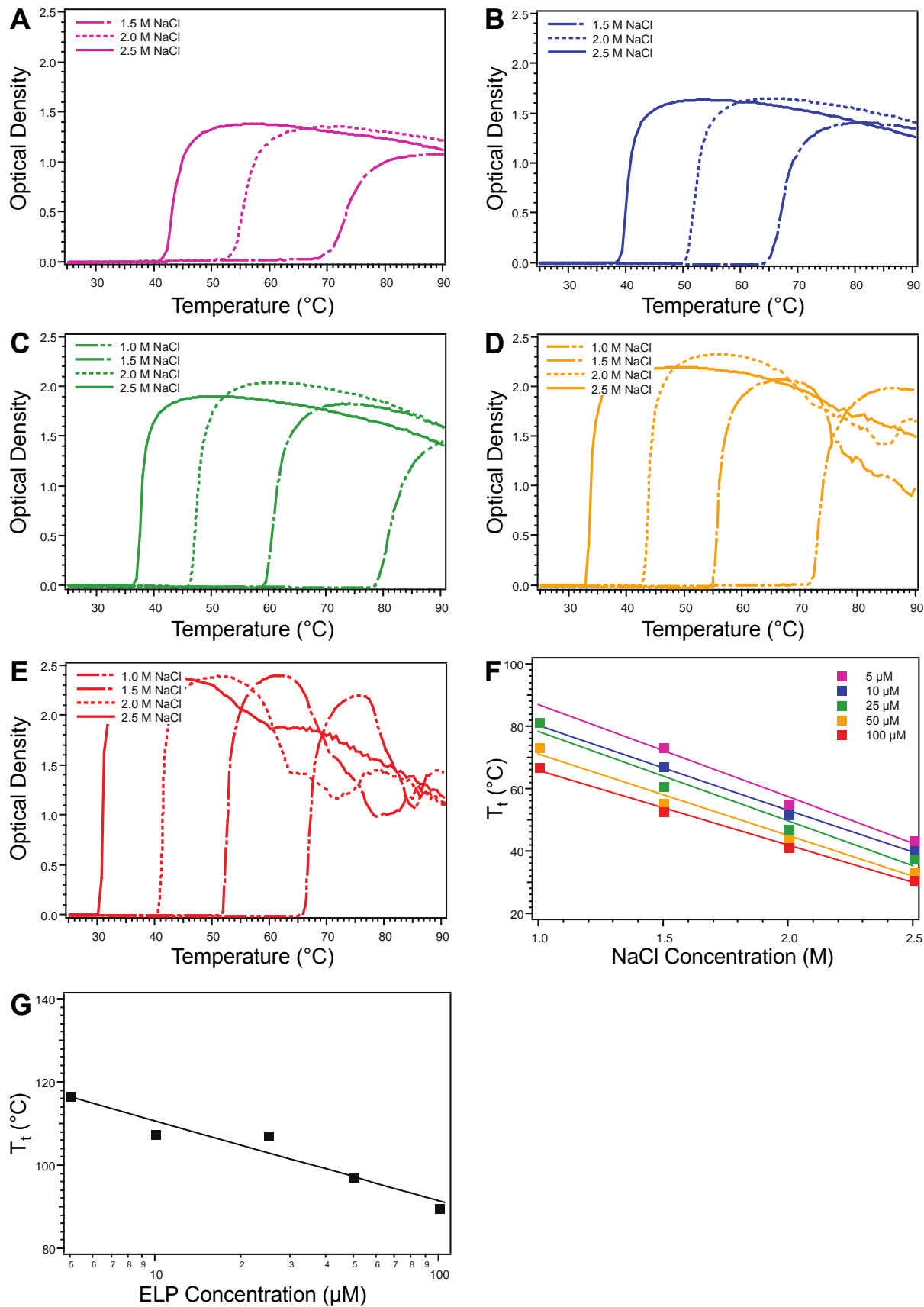


**Figure S3.** Thermal characterization of ELP-S<sub>comp</sub> by temperature-regulated turbidimetry. The T<sub>t</sub> of ELP-S<sub>comp</sub> exceeded the upper thermal limit of the UV-VIS spectrophotometer (90°C). NaCl was added to lower the T<sub>t</sub> such that it could be observed in the measurable temperature range. ELP-S<sub>comp</sub> was characterized by temperature-regulated turbidimetry in 1.0-2.5 M NaCl in PBS at ELP concentrations of A) 5 μM, B) 10 μM, C) 25 μM, D) 50 μM, and E) 100 μM. F) The experimentally measured T<sub>t</sub>s at each ELP concentration (squares) were fit to linear approximations (lines) whose extrapolation defined intercepts that were interpreted as the T<sub>t</sub>s in PBS without NaCl. G) The approximated T<sub>t</sub>s in PBS (squares) at each concentration were fit to a logarithmic relationship (line).

**Table S2.** T<sub>t</sub>s of ELP-S<sub>comp</sub> in NaCl.<sup>1</sup>

ELP concentration (μM)	NaCl concentration (M)			
	1.0	1.5	2.0	2.5
<b>5</b>	NM <sup>2</sup>	73.22	55.41	43.53
<b>10</b>	NM <sup>2</sup>	67.35	52.00	40.19
<b>25</b>	81.42	60.79	47.35	37.89
<b>50</b>	73.32	55.65	43.83	33.73
<b>100</b>	66.94	52.64	41.27	30.89

<sup>1</sup>T<sub>t</sub>s calculated as the temperature corresponding to the maximum of the Gaussian fit of the derivative of the OD, with respect to temperature, reported in °C.

<sup>2</sup>Not measurable (NM) in the temperature range 20-90°C. The T<sub>t</sub> at these conditions exceeded 90°C.

The T<sub>t</sub>s of ELP-S<sub>comp</sub> in NaCl solutions were fit to a linear relationship of T<sub>t</sub>, with respect to NaCl concentration,<sup>3</sup> at a constant ELP concentration as according to Equation S1:

$$T = T_0 + c[M] \quad (\text{S1})$$

where  $T$  is the experimentally measured T<sub>t</sub>,  $T_0$  is the extrapolated T<sub>t</sub> in the absence of salt,  $c$  is a constant of units °C/M and [M] is the molar concentration of NaCl.

**Table S3.** Fit parameters of ELP-S<sub>comp</sub> T<sub>t</sub>s in NaCl.<sup>1</sup>

ELP concentration (μM)	c (°C/M)	T <sub>0</sub> (°C)	r <sup>2</sup>
<b>5</b>	-29.69	116.77	0.987
<b>10</b>	-27.16	107.50	0.994
<b>25</b>	-28.80	107.27	0.970
<b>50</b>	-26.12	97.34	0.982
<b>100</b>	-23.91	89.77	0.994

<sup>1</sup>Parameters according to Equation S1.

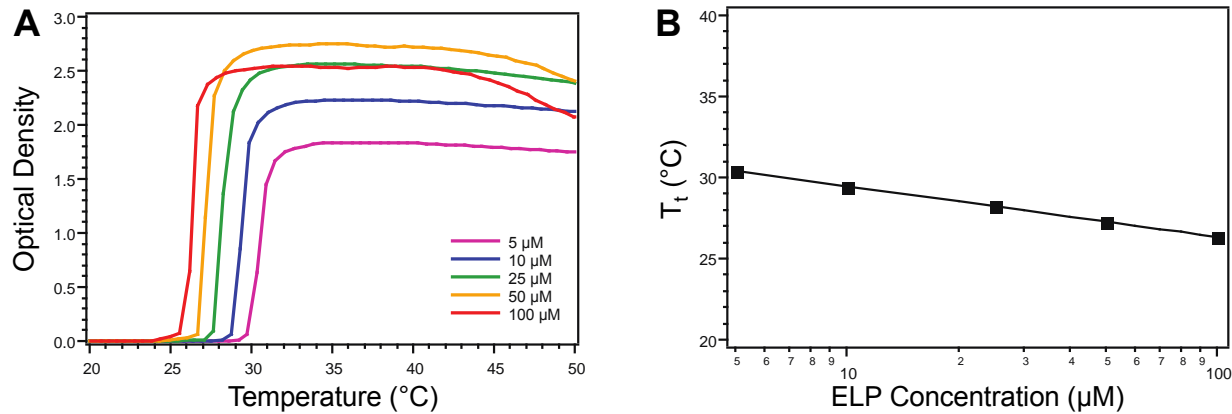


**Figure S4.** Thermal characterization of ELP-V<sub>comp</sub> by temperature-regulated turbidimetry. A) ELP-V<sub>comp</sub> was characterized by temperature-regulated turbidimetry in PBS at ELP concentrations of 5, 10, 25, 50, and 100 μM. B) The T<sub>t</sub>s at each concentration were determined as the temperatures corresponding to the maximum of the Gaussian fit of the derivative of OD with respect to temperature (squares), which were fit to a logarithmic relationship (line).

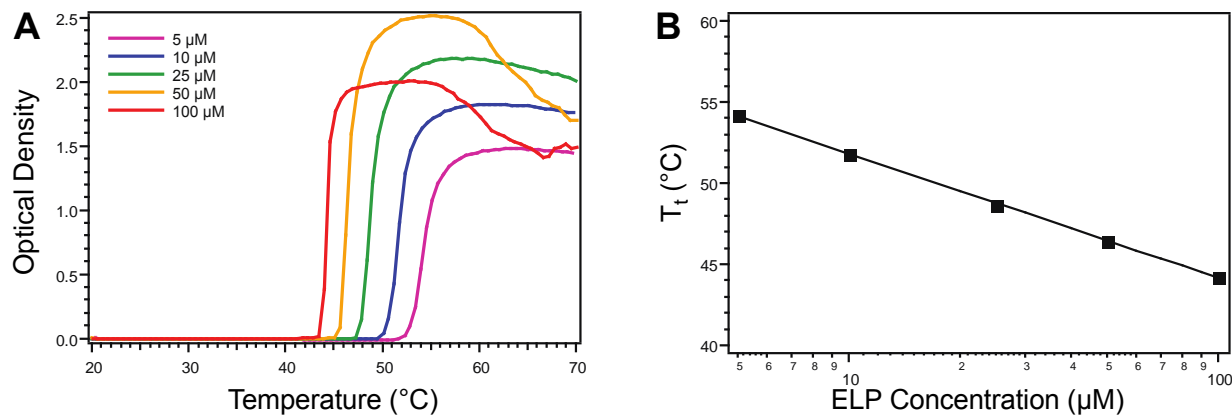


**Figure S5.** Thermal characterization of ELP-SVB<sub>1</sub> by temperature-regulated turbidimetry. A) ELP-SVB<sub>1</sub> was characterized by temperature-regulated turbidimetry in PBS at ELP concentrations of 5, 10, 25, 50, and 100 μM. B) The T<sub>t</sub>s at each concentration were determined as the temperatures corresponding to the maximum of the Gaussian fit of the derivative of OD with respect to temperature (squares), which were fit to a logarithmic relationship (line).

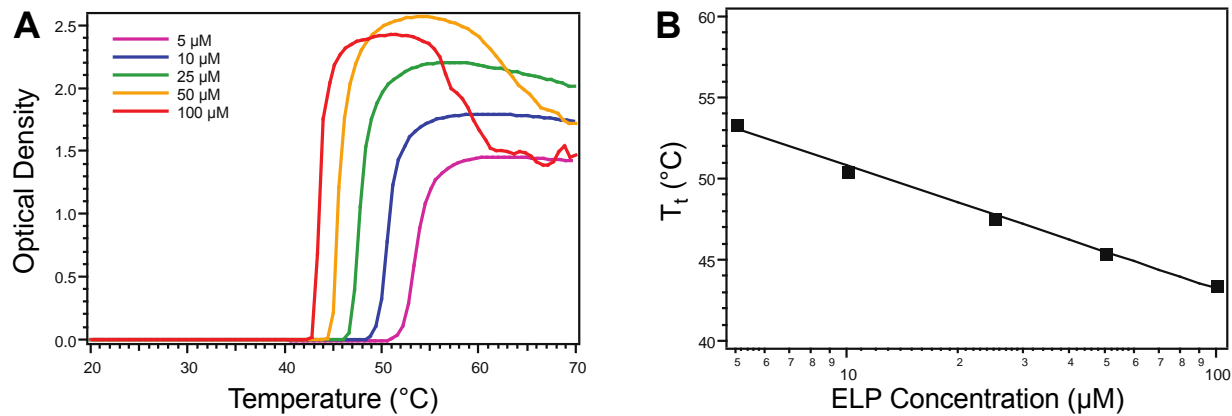


**Figure S6.** Thermal characterization of ELP-SVB<sub>5</sub> by temperature-regulated turbidimetry. A) ELP-SVB<sub>5</sub> was characterized by temperature-regulated turbidimetry in PBS at ELP concentrations of 5, 10, 25, 50, and 100 μM. B) The T<sub>t</sub>s at each concentration were determined as the temperatures corresponding to the maximum of the Gaussian fit of the derivative of OD with respect to temperature (squares), which were fit to a logarithmic relationship (line).

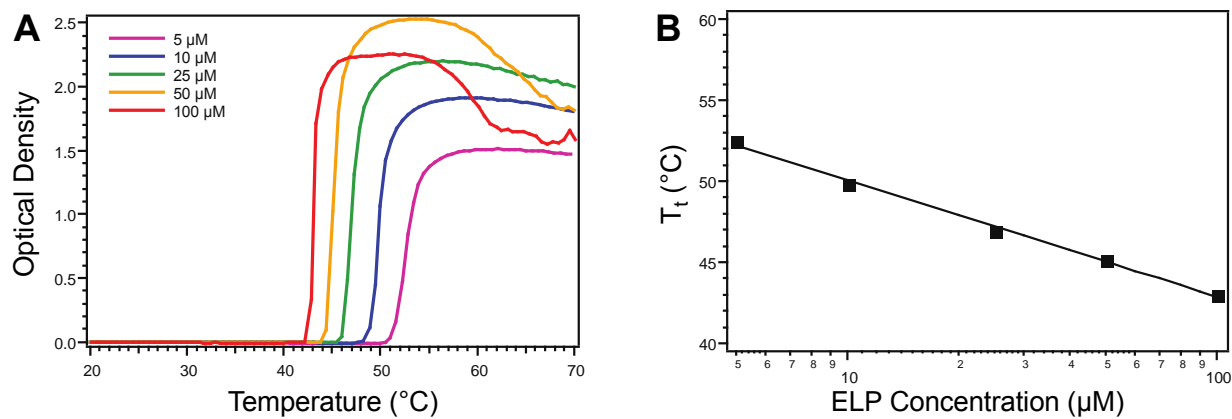


**Figure S7.** Thermal characterization of ELP-SVB<sub>10</sub> by temperature-regulated turbidimetry. A) ELP-SVB<sub>10</sub> was characterized by temperature-regulated turbidimetry in PBS at ELP concentrations of 5, 10, 25, 50, and 100 μM. B) The T<sub>t</sub>s at each concentration were determined as the temperatures corresponding to the maximum of the Gaussian fit of the derivative of OD with respect to temperature (squares), which were fit to a logarithmic relationship (line).

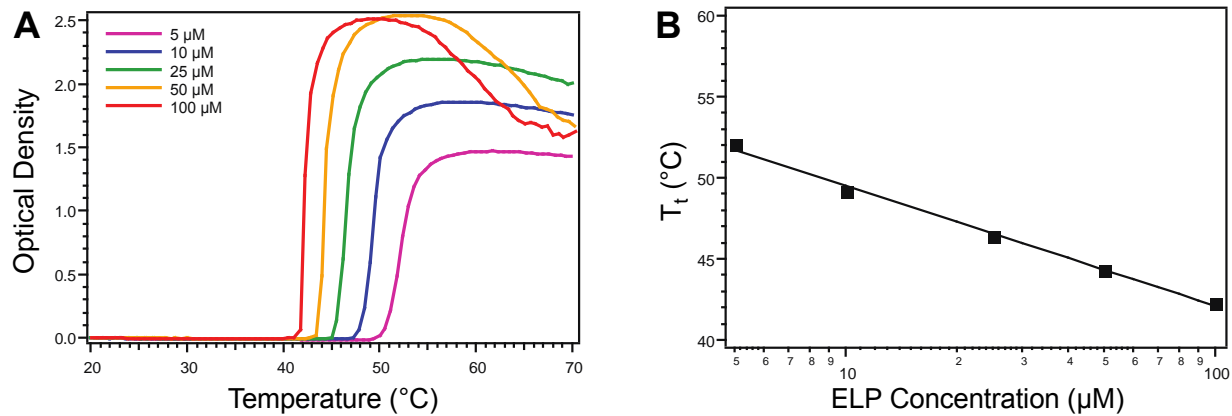


**Figure S8.** Thermal characterization of ELP-SVB<sub>20</sub> by temperature-regulated turbidimetry. A) ELP-SVB<sub>20</sub> was characterized by temperature-regulated turbidimetry in PBS at ELP concentrations of 5, 10, 25, 50, and 100 μM. B) The T<sub>t</sub>s at each concentration were determined as the temperatures corresponding to the maximum of the Gaussian fit of the derivative of OD with respect to temperature (squares), which were fit to a logarithmic relationship (line).

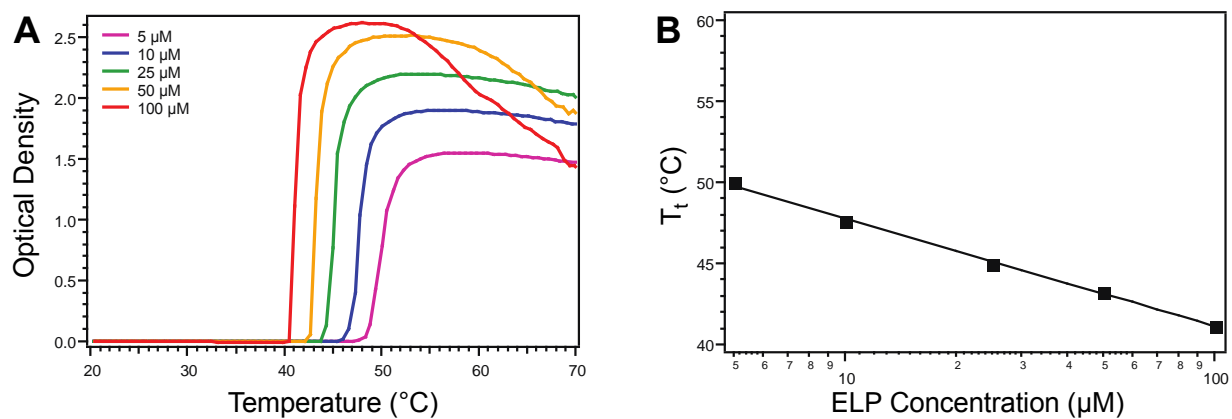


**Figure S9.** Thermal characterization of ELP-SVB<sub>30</sub> by temperature-regulated turbidimetry. A) ELP-SVB<sub>30</sub> was characterized by temperature-regulated turbidimetry in PBS at ELP concentrations of 5, 10, 25, 50, and 100 μM. B) The T<sub>t</sub>s at each concentration were determined as the temperatures corresponding to the maximum of the Gaussian fit of the derivative of OD with respect to temperature (squares), which were fit to a logarithmic relationship (line).

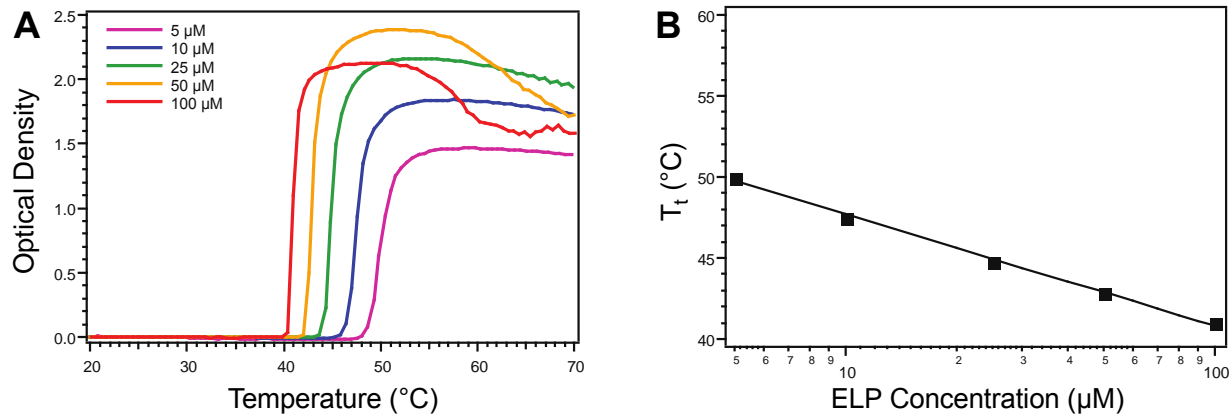


**Figure S10.** Thermal characterization of ELP-SVT<sub>vsv</sub> by temperature-regulated turbidimetry. A) ELP-SVT<sub>vsv</sub> was characterized by temperature-regulated turbidimetry in PBS at ELP concentrations of 5, 10, 25, 50, and 100  $\mu\text{M}$ . B) The  $T_t$ s at each concentration were determined as the temperatures corresponding to the maximum of the Gaussian fit of the derivative of OD with respect to temperature (squares), which were fit to a logarithmic relationship (line).

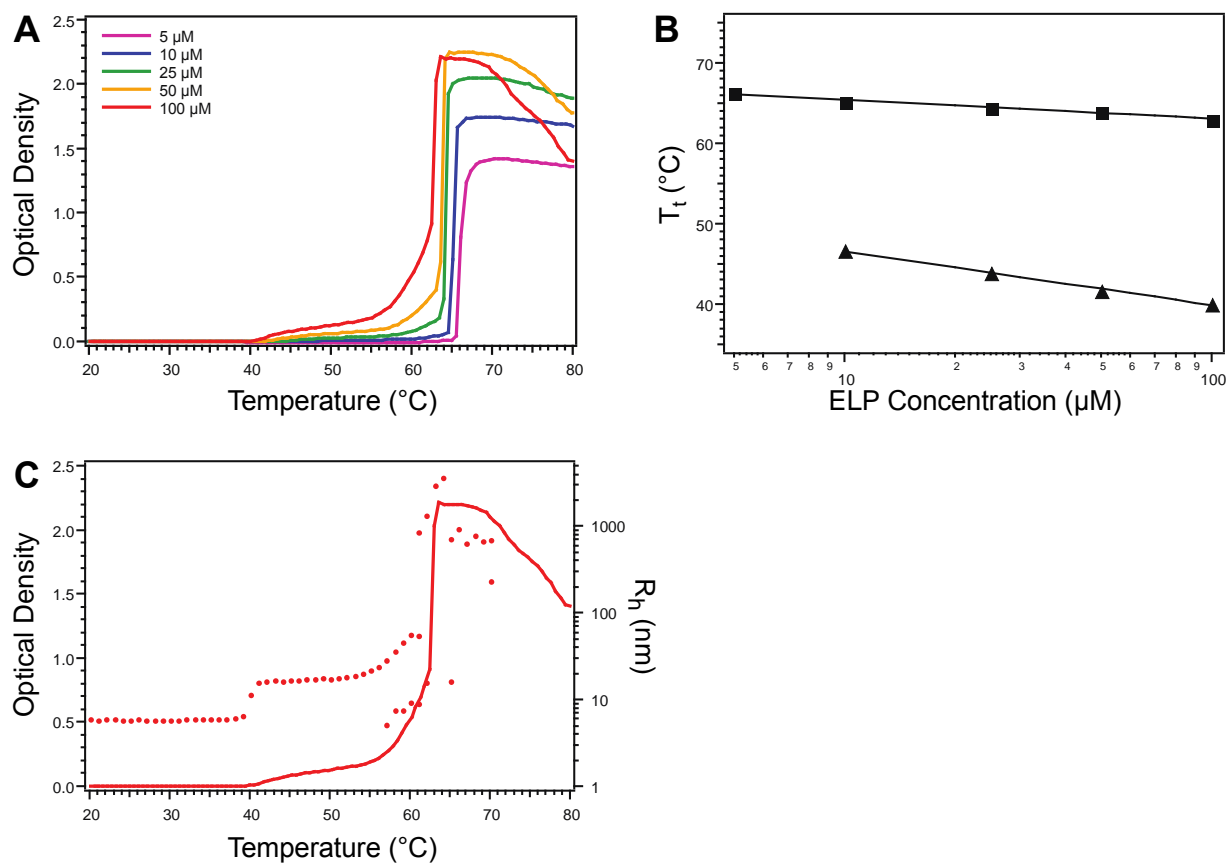


**Figure S11.** Thermal characterization of ELP-SVT<sub>svs</sub> by temperature-regulated turbidimetry and DLS. A) ELP-SVT<sub>svs</sub> was characterized by temperature-regulated turbidimetry in PBS at ELP

concentrations of 5, 10, 25, 50, and 100  $\mu\text{M}$ . B) The  $T_t$ s at each concentration were determined as the temperatures corresponding to the maximum of the Gaussian fit of the derivative of OD with respect to temperature (squares), which were fit to a logarithmic relationship (line). The CMTs at each concentration were approximated as the temperatures corresponding to the positive divergences of OD from baseline (triangles), which were fit to a logarithmic relationship (line). Turbidimetry was not sensitive enough to determine the CMT below 10  $\mu\text{M}$ . C) DLS measurement of  $R_h$  (dots, right ordinate) at 100  $\mu\text{M}$  corroborated the self-assembly with respect to temperature as determined by turbidimetry (line, left ordinate).

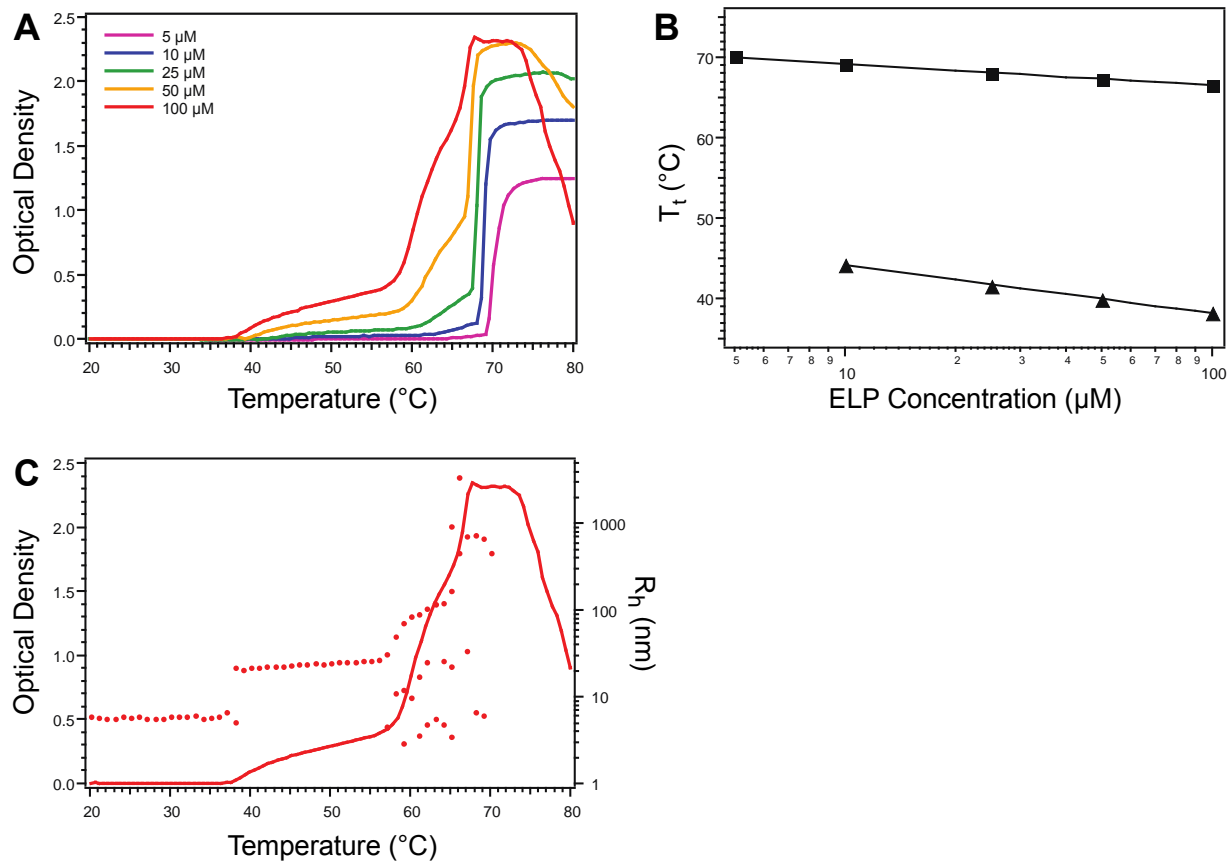


**Figure S12.** Thermal characterization of ELP-SVD<sub>Sv</sub> by temperature-regulated turbidimetry and DLS. A) ELP-SVD<sub>Sv</sub> was characterized by temperature-regulated turbidimetry in PBS at ELP concentrations of 5, 10, 25, 50, and 100  $\mu\text{M}$ . B) The  $T_t$ s at each concentration were determined as the temperatures corresponding to the maximum of the Gaussian fit of the derivative of OD with respect to temperature (squares), which were fit to a logarithmic relationship (line). The CMTs at each concentration were approximated as the temperatures corresponding to the positive divergences of OD from baseline (triangles), which were fit to a logarithmic relationship (line). Turbidimetry was not sensitive enough to determine the CMT below 10  $\mu\text{M}$ . C) DLS measurement of  $R_h$  (dots, right ordinate) at 100  $\mu\text{M}$  corroborated the self-assembly with respect to temperature as determined by turbidimetry (line, left ordinate).

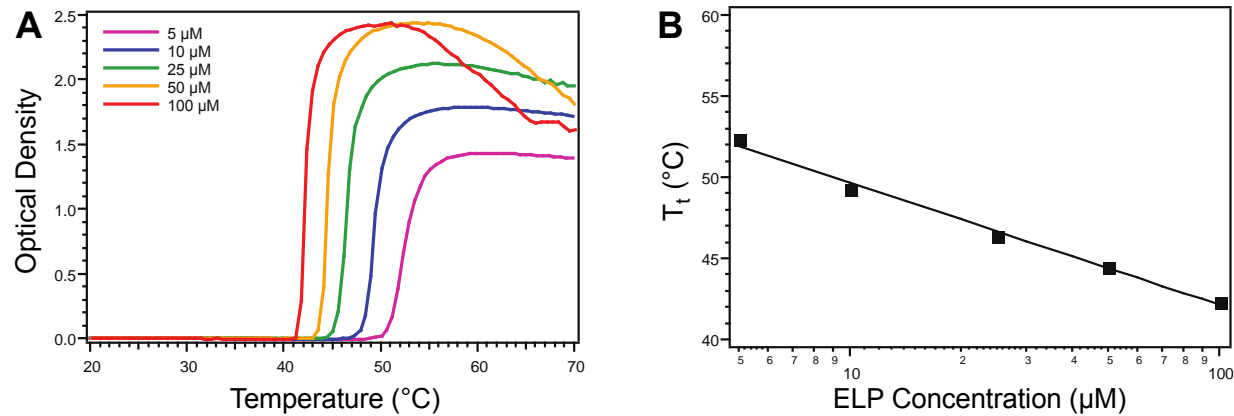


**Figure S13.** Thermal characterization of ELP-SVG<sub>L</sub> by temperature-regulated turbidimetry. A) ELP-SVG<sub>L</sub> was characterized by temperature-regulated turbidimetry in PBS at ELP concentrations of 5, 10, 25, 50, and 100 μM. B) The T<sub>t</sub>s at each concentration were determined as the temperatures corresponding to the maximum of the Gaussian fit of the derivative of OD with respect to temperature (squares), which were fit to a logarithmic relationship (line).

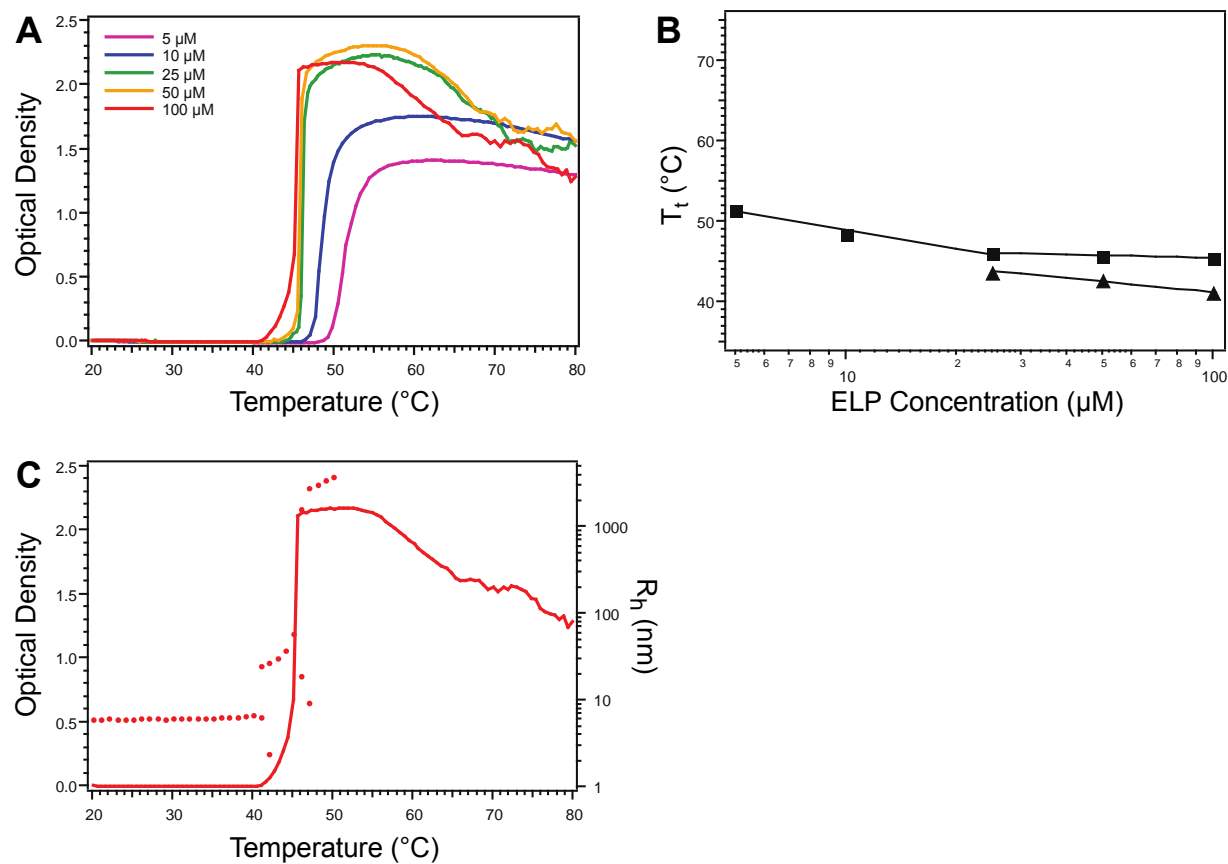


**Figure S14.** Thermal characterization of ELP-SVG<sub>I</sub> by temperature-regulated turbidimetry and DLS. A) ELP-SVG<sub>I</sub> was characterized by temperature-regulated turbidimetry in PBS at ELP

concentrations of 5, 10, 25, 50, and 100  $\mu\text{M}$ . B) The  $T_t$ s at each concentration were determined as the temperatures corresponding to the maximum of the Gaussian fit of the derivative of OD with respect to temperature (squares), which were fit to two separate logarithmic relationships for 5-25  $\mu\text{M}$  and 25-100  $\mu\text{M}$  (line). The CMTs at each concentration were approximated as the temperatures corresponding to the positive divergences of OD from baseline (triangles), which were fit to a logarithmic relationship (line). No CMT was evident below 25  $\mu\text{M}$  by turbidimetry, which was supported by the difference in slope of the logarithmic fit to the measured  $T_t$ s above and below 25  $\mu\text{M}$ . C) DLS measurement of  $R_h$  (dots, right ordinate) at 100  $\mu\text{M}$  corroborated the self-assembly with respect to temperature as determined by turbidimetry (line, left ordinate).

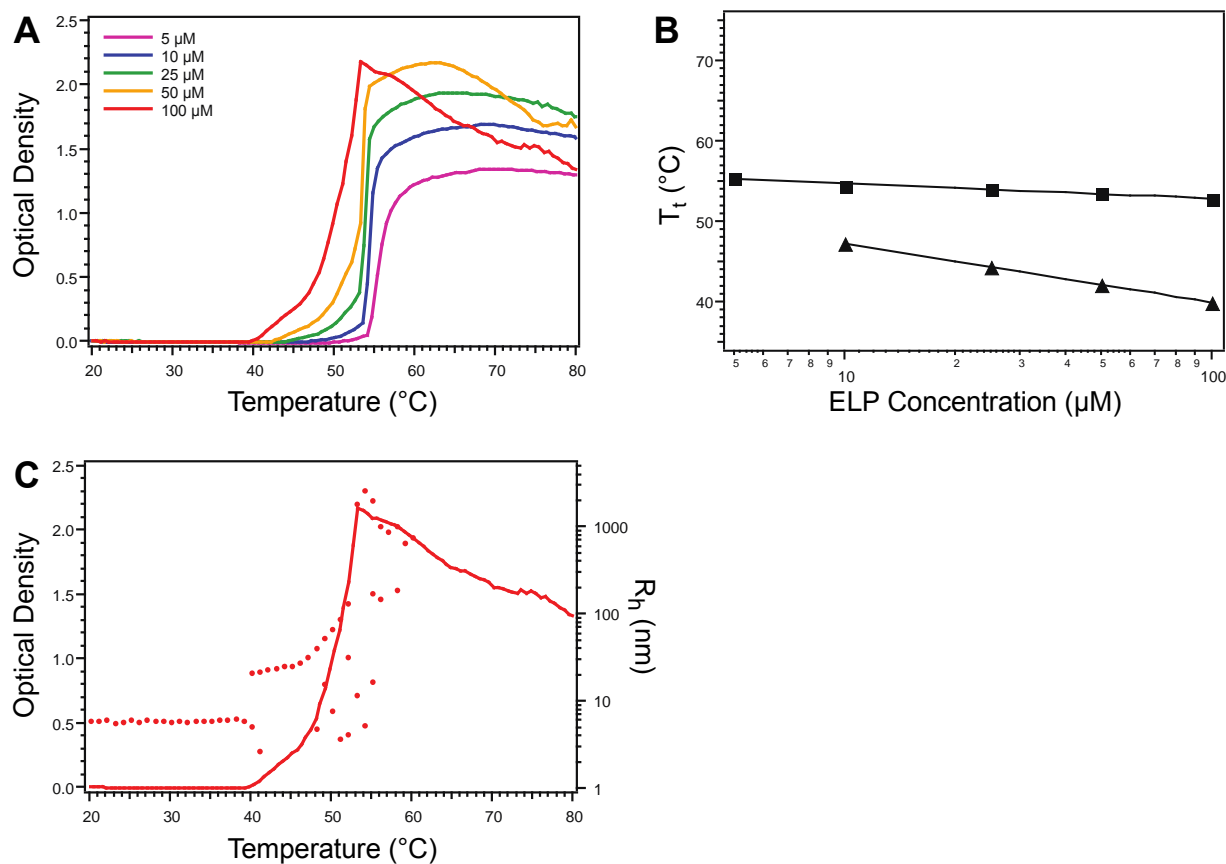


**Figure S15.** Thermal characterization of ELP-SVG<sub>H</sub> by temperature-regulated turbidimetry and DLS. A) ELP-SVG<sub>H</sub> was characterized by temperature-regulated turbidimetry in PBS at ELP concentrations of 5, 10, 25, 50, and 100  $\mu\text{M}$ . B) The  $T_t$ s at each concentration were determined as the temperatures corresponding to the maximum of the Gaussian fit of the derivative of OD with respect to temperature (squares), which were fit to a logarithmic relationship (line). The CMTs at each concentration were approximated as the temperatures corresponding to the positive divergences of OD from baseline (triangles), which were fit to a logarithmic relationship (line). Turbidimetry was not sensitive enough to determine the CMT below 25  $\mu\text{M}$ . C) DLS measurement of  $R_h$  (dots, right ordinate) at 100  $\mu\text{M}$  corroborated the self-assembly with respect to temperature as determined by turbidimetry (line, left ordinate).

**Table S4.** ELP T<sub>t</sub>s.<sup>1</sup>

ELP	ELP concentration ( $\mu\text{M}$ )				
	5	10	25	50	100
S <sub>comp</sub> <sup>2</sup>	116.77	107.50	107.27	97.34	89.77
V <sub>comp</sub>	38.84	36.93	34.77	33.54	31.93
SVB <sub>1</sub>	54.23	51.80	48.66	46.45	44.24
SVB <sub>5</sub>	53.40	50.52	47.60	45.42	43.46
SVB <sub>10</sub>	52.50	49.83	46.93	45.17	42.99
SVB <sub>20</sub>	52.08	49.14	46.40	44.29	42.30
SVB <sub>30</sub>	49.97	47.62	44.97	43.26	41.17
SVT <sub>VSV</sub>	49.94	47.52	44.82	42.86	40.95
SVT <sub>SVS</sub>	66.20	65.12	64.50	63.91	62.95
SVD <sub>SV</sub>	70.07	69.10	68.03	67.39	66.50
SVG <sub>L</sub>	52.33	49.34	46.42	44.46	42.30
SVG <sub>I</sub>	51.45	48.39	46.04	45.71	45.41
SVG <sub>H</sub>	55.37	54.39	54.09	53.44	52.80

<sup>1</sup>T<sub>t</sub>s calculated as the temperature corresponding to the maximum of the Gaussian fit of the derivative of OD, with respect to temperature, reported in °C. This T<sub>t</sub> corresponded to the phase transition of ELP into unstable micron-scale coacervates, from either a unimer or micelle state.

<sup>2</sup>T<sub>t</sub>s of ELP-S<sub>comp</sub> were determined from extrapolation of T<sub>t</sub>s measured in NaCl dilutions (see Table S2 and S3).

**Table S5.** ELP CMTs.<sup>1</sup>

ELP	ELP concentration ( $\mu\text{M}$ )			
	10	25	50	100
SVT <sub>SVS</sub>	46.62	43.92	41.72	40.00
SVD <sub>SV</sub>	44.22	41.57	39.92	38.22
SVG <sub>I</sub>	NM <sup>2</sup>	43.67	42.67	41.07
SVG <sub>H</sub>	47.18	44.37	42.14	39.87

<sup>1</sup>For those ELPs exhibiting temperature-triggered self-assembly, the CMT, corresponding to the temperature at which the unimer-to-micelle transition occurred, was approximated as the temperature at which the OD deviated positively from baseline, reported in °C. Due to the limited sensitivity of turbidimetry to self-assembled nanoparticles at low concentrations, approximations were not made at 5  $\mu\text{M}$ .

<sup>2</sup>No CMT was evident for measurement of ELP-SVG<sub>I</sub> at concentrations of 10  $\mu\text{M}$  and lower.

The ELP T<sub>t</sub> (or CMT) exhibited a logarithmic relationship to concentration<sup>4</sup> as described by Equation S2:

$$T_t = b + m \ln C \quad (\text{S2})$$

which is a simplification of the relationship that more precisely describes the dependence of T<sub>t</sub> on the ELP's sequence, size, and concentration,<sup>4</sup> as described in Equation S3:

$$T_t = T_{t,c} + \frac{k}{L} \ln \frac{C_c}{C} \quad (S3)$$

where L is the ELP length in pentapeptides, k is a constant of units  $^{\circ}\text{C} \cdot \text{pentapeptides}$ , and  $T_{t,c}$  and  $C_c$  are a critical temperature and concentration, respectively, that are determined at a limit of high concentration and high ELP length, which is unique to each ELP sequence. The length was conserved over the family of ELPs investigated here, such that  $T_{t,c}$ ,  $C_c$ , and k could not be experimentally determined. Therefore the simplified Equation S2 was used to fit the relationship between ELP concentration and  $T_t$  (or CMT).

**Table S6.** Fit parameters of ELP  $T_{ts}$ .<sup>1</sup>

ELP	<i>m</i> ( $^{\circ}\text{C}$ )	<i>b</i> ( $^{\circ}\text{C}$ )	<i>r</i> <sup>2</sup>
<b>S<sub>comp</sub></b> <sup>2</sup>	-8.33	129.78	0.928
<b>V<sub>comp</sub></b>	-2.27	42.30	0.996
<b>SVB<sub>1</sub></b>	-3.34	59.51	0.999
<b>SVB<sub>5</sub></b>	-3.29	58.37	0.996
<b>SVB<sub>10</sub></b>	-3.12	57.25	0.996
<b>SVB<sub>20</sub></b>	-3.21	56.90	0.995
<b>SVB<sub>30</sub></b>	-2.89	54.45	0.998
<b>SVT<sub>VSV</sub></b>	-2.98	54.54	0.998
<b>SVT<sub>SVS</sub></b>	-1.01	67.70	0.980
<b>SVD<sub>SV</sub></b>	-1.17	71.87	0.997
<b>SVG<sub>L</sub></b>	-3.29	57.25	0.994
<b>SVG<sub>I</sub></b>	-3.32 <sup>3</sup>	56.53 <sup>3</sup>	0.976 <sup>3</sup>
	-0.45 <sup>4</sup>	47.48 <sup>4</sup>	0.999 <sup>4</sup>
<b>SVG<sub>H</sub></b>	-0.80	56.51	0.967

<sup>1</sup>Parameters according to Equation S2, fit to  $T_{ts}$  measured at 5-100  $\mu\text{M}$ .

<sup>2</sup>Fit based on  $T_{ts}$  determined from extrapolation of  $T_{ts}$  measured in NaCl (see Table S2 and S3).

<sup>3</sup>Fit to  $T_{ts}$  at concentrations 5-25  $\mu\text{M}$ .

<sup>4</sup>Fit to  $T_{ts}$  at concentrations 25-100  $\mu\text{M}$ .

**Table S7.** Fit parameters of ELP CMTs.<sup>1</sup>

ELP	<i>m</i> ( $^{\circ}\text{C}$ )	<i>b</i> ( $^{\circ}\text{C}$ )	<i>r</i> <sup>2</sup>
<b>SVT<sub>SVS</sub></b>	-2.91	53.27	0.998
<b>SVD<sub>SV</sub></b>	-2.59	50.09	0.998
<b>SVG<sub>I</sub></b>	-1.88 <sup>2</sup>	49.81 <sup>2</sup>	0.983 <sup>2</sup>
<b>SVG<sub>H</sub></b>	-3.18	54.53	0.999

<sup>1</sup>Parameters according to Equation S2, fit to CMTs approximated at 10-100  $\mu\text{M}$ .

<sup>2</sup>Fit to CMTs approximated at 25-100  $\mu\text{M}$ .

**Table S8.** Refractive index increment of self-assembling ELPs.

ELP	$\text{dn}/\text{dc}$ (mL/mg)	<i>r</i> <sup>2</sup>
-----	-------------------------------	-----------------------

<b>SVT<sub>SVS</sub></b>	$1.797764 \times 10^{-4}$	0.999
<b>SVD<sub>SV</sub></b>	$1.653665 \times 10^{-4}$	0.999
<b>SVG<sub>H</sub></b>	$1.729193 \times 10^{-4}$	0.999
<b>SVG<sub>I</sub></b>	$1.749068 \times 10^{-4}$	0.985

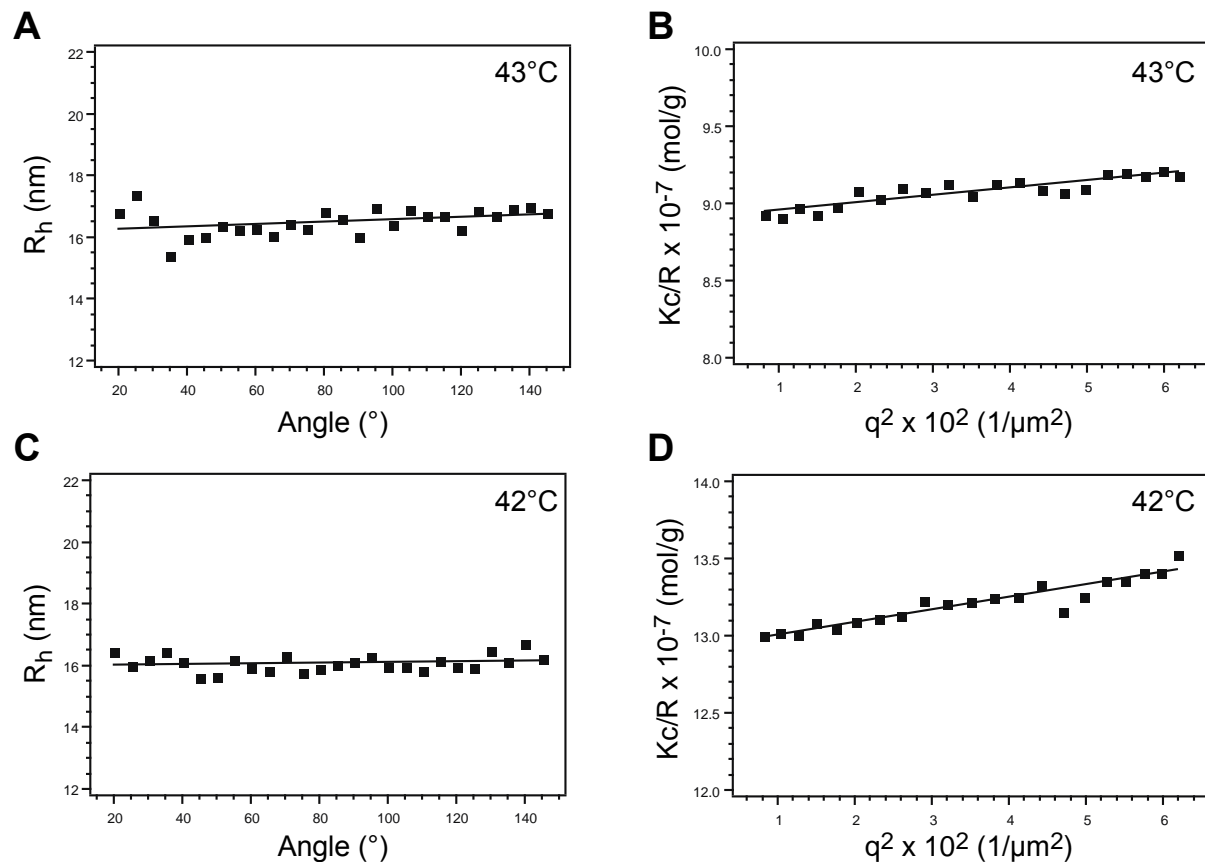


**Figure S16.** Characterization of ELP-SVT<sub>SVS</sub> by SLS and DLS. A)  $R_h$  was determined from DLS measurements and B)  $R_g$  and MW was determined from SLS measurements of 100  $\mu\text{M}$  solution at 43°C. C)  $R_h$  was determined from DLS measurements and D)  $R_g$  and MW was determined from SLS measurements of 100  $\mu\text{M}$  solution at 42°C, 2°C above the CMT of ELP-SVT<sub>SVS</sub>. Markers represent individual measurements while solid lines represent linear fits to the data.

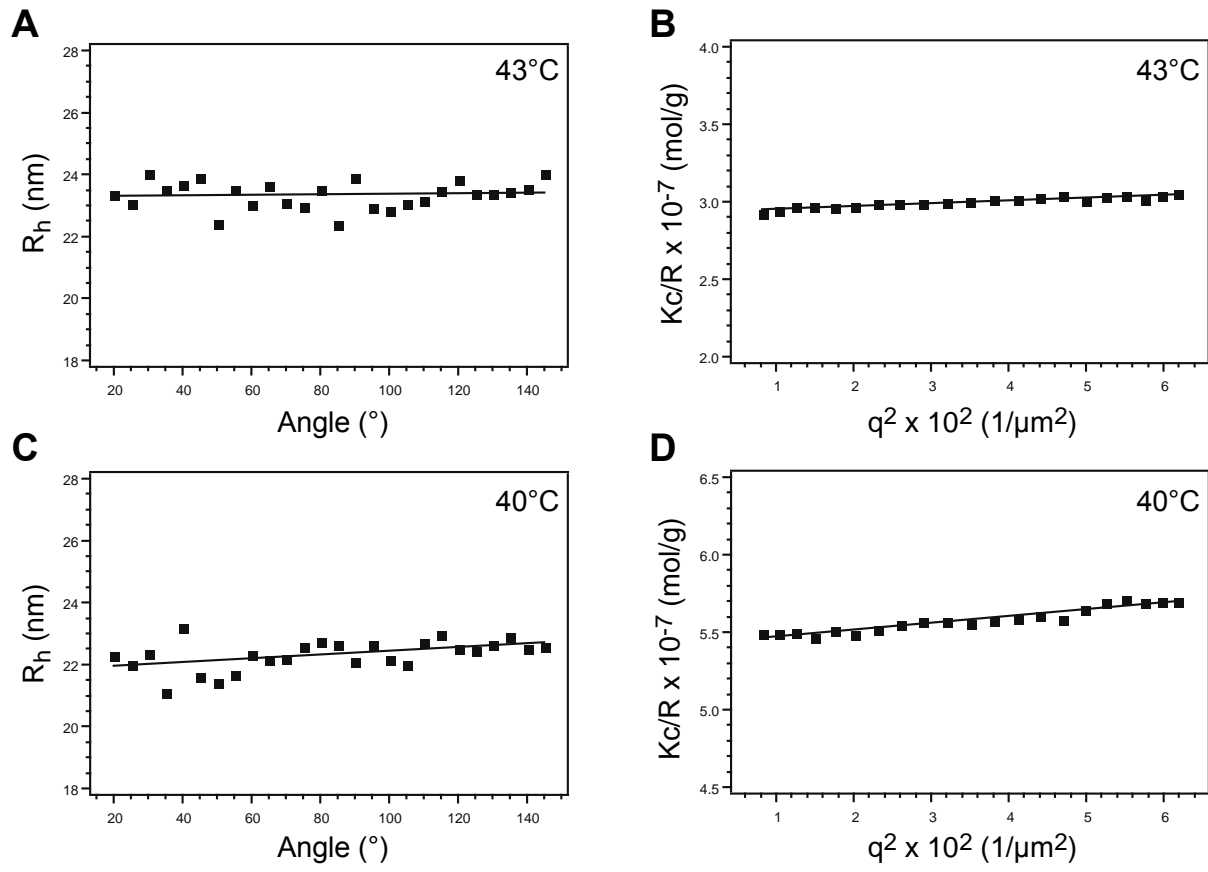


**Figure S17.** Characterization of ELP-SVD<sub>SV</sub> by SLS and DLS. A)  $R_h$  was determined from DLS measurements and B)  $R_g$  and MW was determined from SLS measurements of 100  $\mu\text{M}$  solution at 43°C. C)  $R_h$  was determined from DLS measurements and D)  $R_g$  and MW was determined from SLS measurements of 100  $\mu\text{M}$  solution at 40°C, 2°C above the CMT of ELP-SVD<sub>SV</sub>. Markers represent individual measurements while solid lines represent linear fits to the data.

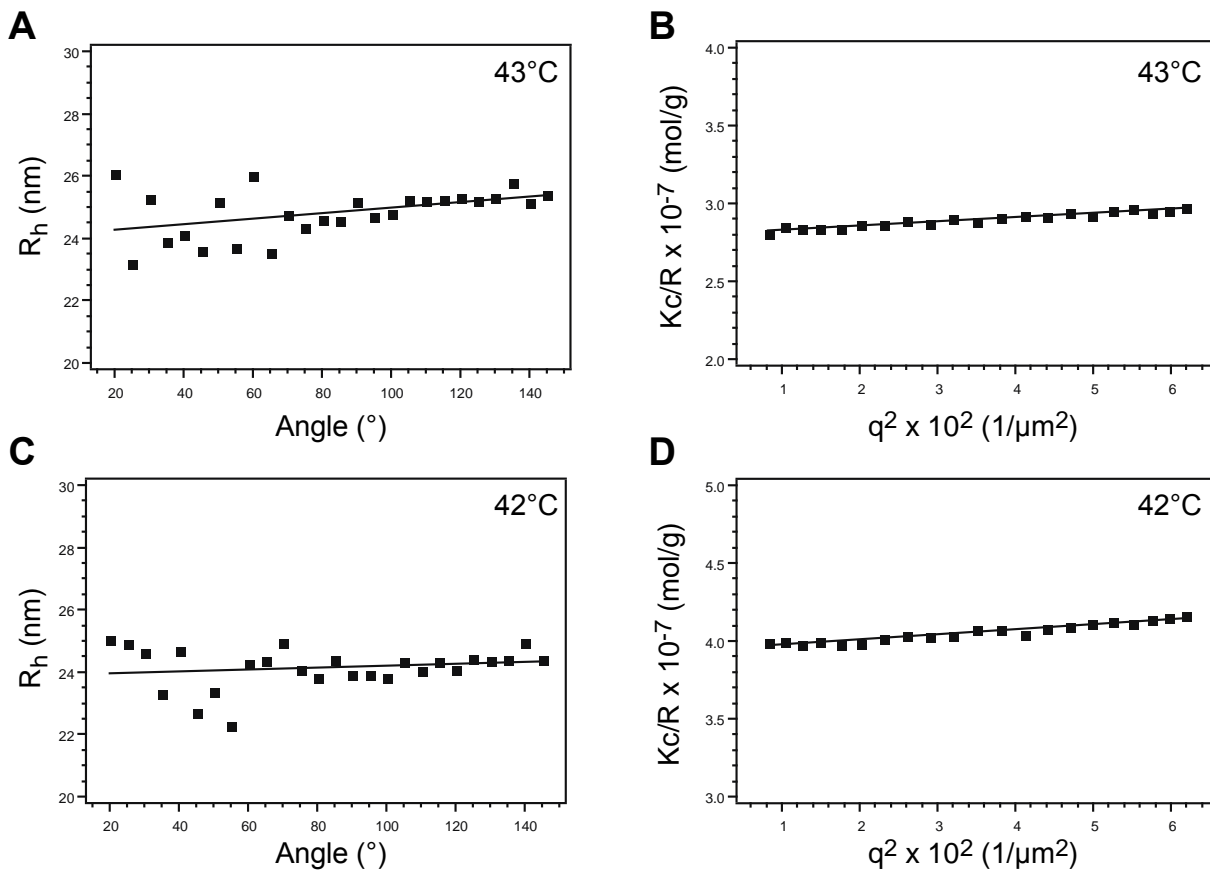


**Figure S18.** Characterization of ELP-SVG<sub>H</sub> by SLS and DLS. A)  $R_h$  was determined from DLS measurements and B)  $R_g$  and MW was determined from SLS measurements of 100  $\mu\text{M}$  solution at 43°C. C)  $R_h$  was determined from DLS measurements and D)  $R_g$  and MW was determined from SLS measurements of 100  $\mu\text{M}$  solution at 42°C, 2°C above the CMT of ELP-SVG<sub>H</sub>. Markers represent individual measurements while solid lines represent linear fits to the data.

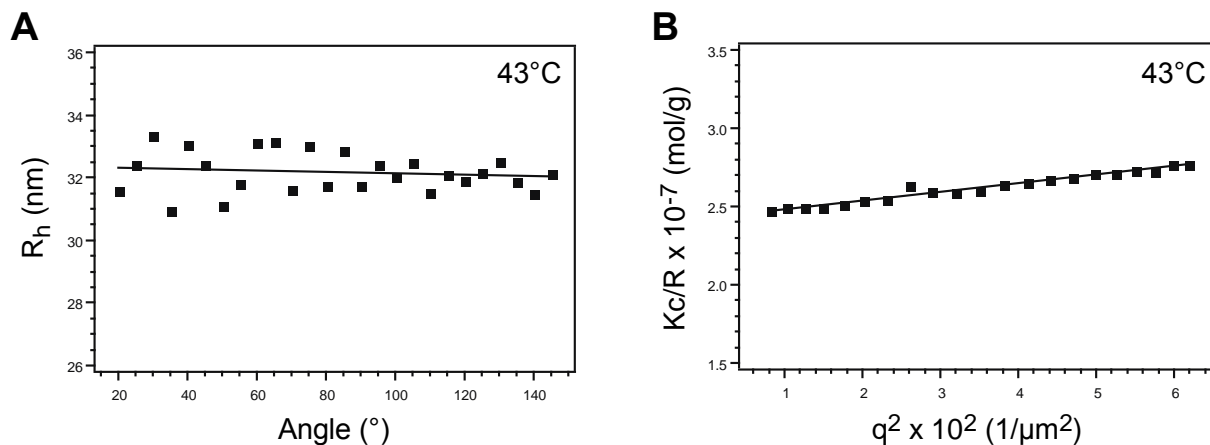


**Figure S19.** Characterization of ELP-SVG<sub>I</sub> by SLS and DLS. A) R<sub>h</sub> was determined from DLS measurements and B) R<sub>g</sub> and MW was determined from SLS measurements of 100 μM solution at 43°C, 2°C above the CMT of ELP-SVG<sub>I</sub>. Markers represent individual measurements while solid lines represent linear fits to the data.

**Table S9.** Summary of SLS and DLS characterization of ELP self-assembly at 43°C.

ELP	R <sub>g</sub> (nm)	R <sub>h</sub> (nm)	ρ (R <sub>g</sub> /R <sub>h</sub> )	MW (g/mol)	N <sub>agg</sub>
SVT <sub>SVS</sub>	12.7 (±5.9%)	16.2	0.78	1.122 x 10 <sup>6</sup> (±0.25%)	23
SVD <sub>SV</sub>	13.8 (±4.2%)	23.3	0.59	3.408 x 10 <sup>6</sup> (±0.21%)	70
SVG <sub>H</sub>	17.0 (±2.8%)	24.1	0.70	3.564 x 10 <sup>6</sup> (±0.21%)	73
SVG <sub>I</sub>	26.1 (±2.0%)	32.4	0.81	4.118 x 10 <sup>6</sup> (±0.35%)	85

**Table S10.** Summary of SLS and DLS characterization of ELP self-assembly at 2°C above the CMT.<sup>1</sup>

ELP	R <sub>g</sub> (nm)	R <sub>h</sub> (nm)	ρ (R <sub>g</sub> /R <sub>h</sub> )	MW (g/mol)	N <sub>agg</sub>
SVT <sub>SVS</sub>	13.7 (±4.0%)	16.0	0.86	7.735 x 10 <sup>6</sup> (±0.20%)	16
SVD <sub>SV</sub>	15.7 (±3.4%)	21.8	0.72	1.842 x 10 <sup>6</sup> (±0.22%)	38
SVG <sub>H</sub>	15.9 (±3.1%)	23.9	0.67	2.537 x 10 <sup>6</sup> (±0.20%)	52
SVG <sub>I</sub>	26.1 (±2.0%)	32.4	0.81	4.118 x 10 <sup>6</sup> (±0.35%)	85

<sup>1</sup>Measurements were made at 2°C above the CMT: ELP-SVT<sub>SVS</sub> at 42°C, ELP-SVD<sub>SV</sub> at 40°C, ELP-SVG<sub>H</sub> at 42°C, and ELP-SVG<sub>I</sub> at 43°C.

## A) ELP-V-SVB<sub>1</sub>-S

## B) ELP-V-SVB<sub>5</sub>-S

### C) ELP-V-SVB<sub>10</sub>-S

M G V G V P G V G V P G V G V P G V G V P G V G V P G V G V P G V G V  
atg ggc gtg ggt gtt ccg ggc gta ggt gtc cca ggt gtg ggc gta ccg ggc gtt ggt gtt cct ggt gtc ggc gtc gtc ggc gtc ggt gtt gtt  
P G V G V P G V G V P G V G V P G V G V P G V G V P G V G V P G V G V  
ccg ggc gta ggt gtc cca ggt gtg ggc gta ccg ggc gtt ggt gtt cct ggt gtc ggc gtc gtc ggc gtc ggt gtt ccg ggc gta ggt gtc  
P G V G V P G V G V P G V G V P G V G V P G V G V P G V G V P G V G V  
cca ggt gtg ggc gta ccg ggc gtt ggt gtt cct ggt gtc ggc gtc ggc gtt ggt gtt ccg ggc gta ggt gtc cca ggt gtg ggc gta  
P G V G V P G V G V P G V G V P G V G V P G V G V P G V G V P G V G V  
ccg ggc gtt ggt gtt cct ggt gtc ggc gtc ggc gtt ggt ccg ggc gta ggt gtc cca ggt gtg ggc gta ccg ggc gtt ggt gtt  
P G V G V P G V G V P G V G V P G V G V P G V G V P G V G V P G V G V  
cct ggt gtc ggc gtc ggc gtt ggt ccg ggc gta ggt gtc cca ggt gtg ggc gta ccg ggc gtt ggt gtt cct ggt gtc ggc gtc  
P G V G V P G V G V P G V G V P G V G V P G V G V P G V G V P G V G V  
ccg ggc gtc gtc gca ggt gtg ggc gta ccg ggc gtt ggt gtt cct ggt gtc ggc gtc gtc ggc ggt gtt ccg ggc tct ggt gtc  
P G S G V P G S G V P G S G V P G S G V P G S G V P G S G V P G S G V  
cca ggt tcc ggc gta ccg ggc agc ggt gtt cct ggt tct ggc gtc ggc gtt ccg ggc gta ccg ggc gtt ggt gtt cct ggt gtc  
P G S G V P G S G V P G S G V P G S G V P G S G V P G S G V P G S G V  
ccg ggc agc ggt gtt cct ggt tct ggc gtc gca ggt gtg ggc gta ccg ggc gtt ggt gtt cct ggt gtc ggc gtc gtc ggt gtt  
P G V G V P G V G V P G V G V P G V G V P G V G V P G V G V P G V G V  
cct ggt gtc ggc gtc gtc ggc gtt ggt ccg ggc gta ggt gtc cca ggt gtg ggc gta ccg ggc gtt ggt gtt cct ggt gtc ggc  
P G S G V P G S G V P G S G V P G S G V P G S G V P G S G V P G S G V  
ccg ggc agc ggt gtt cct ggt tct ggt gtc cca ggt tcc ggc gta ccg ggc agc ggt gtt cct ggt tct ggc gtc gtc ggc agc  
P G S G V P G S G V P G S G V P G S G V P G S G V P G S G V P G S G V  
ccg ggc tct ggt gtc cca ggt tcc ggc gta ccg ggc agc ggt gtt cct ggt tct ggc gtc gtc cca ggt gtg ggc gta ggt gtc  
P G V G V P G V G V P G V G V P G V G V P G V G V P G V G V P G V G V  
cca ggt gtg ggc gta ccg ggc gtt ggt gtt cct ggt gtc ggc gtc ggc gtt ggt gtt ccg ggc gta ggt gtc cca ggt gtg ggc  
P G V G V P G V G V P G V G V P G V G V P G V G V P G V G V P G V G V  
ccg ggc gtt ggt gtt cct ggt gtc ggc gtc ggc agc ggt gtt ccg ggc gtc gtc cca ggt tcc ggc gta ccg ggc agc ggt gtt  
P G S G V P G S G V P G S G V P G S G V P G S G V P G S G V P G S G V  
cct ggt tct ggc gtc gcg ggc agc ggt gtt ccg ggc tct ggt gtc cca ggt tcc ggc gta ccg ggc agc ggt gtt cct ggt tct  
P G S G V P G S G V P G S G V P G S G V P G S G V P G S G V P G S G V  
ccg ggc agc ggt gtt cct ggt tct ggc gtc cca ggt tcc ggc gta ccg ggc agc ggt gtt cct ggt tct ggc gtc gtc ggc agc  
P G S G V P G S G V P G S G V P G S G V P G S G V P G S G V P G S G V  
ccg ggc tct ggt gtc cca ggt tcc ggc gta ccg ggc agc ggt gtt cct ggt tct ggc gtc gtc cca ggt gtg ggc gta ggt gtc  
P G S G V P G S G V P G S G V P G S G V P G S G V P G S G V P G S G V  
cca ggt tcc ggc gta ccg ggc agc ggt gtt cct ggt tct ggc gtc gtc cca ggt tcc ggc gta ccg ggc agc ggt gtt cct ggt  
P G S G V P G S G V P G S G V P G S G V P G S G V P G S G V P G S G V  
ccg ggc agc ggt gtt cct ggt tct ggc gtc cca ggt tcc ggc gta ccg ggc agc ggt gtt cct ggt tct ggc gtc gtc cca ggt  
P G S G V P G S G V P G S G V P G S G V P G S G V P G S G V P G S G V  
cct ggt tct ggc gtc cca ggt tcc ggc gta ccg ggc agc ggt gtt cct ggt tct ggc gtc gtc cca ggt gtg ggc gta ggt gtc  
P G Y  
ccg ggc tac

**Figure S20.** DNA and polypeptide sequences of blocky interface ELPs. ELP composition and length was equivalent to all other ELPs with various block architectures.

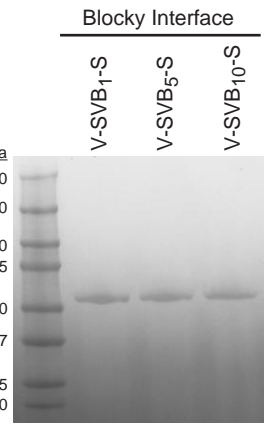


**Figure S21.** Evaluation of blocky interface ELP size and purity by SDS-PAGE and CuCl<sub>2</sub> staining. These ELPs ran slightly higher than their expected MW of 48.66 kDa, which has been previously reported for other ELPs.<sup>2</sup>

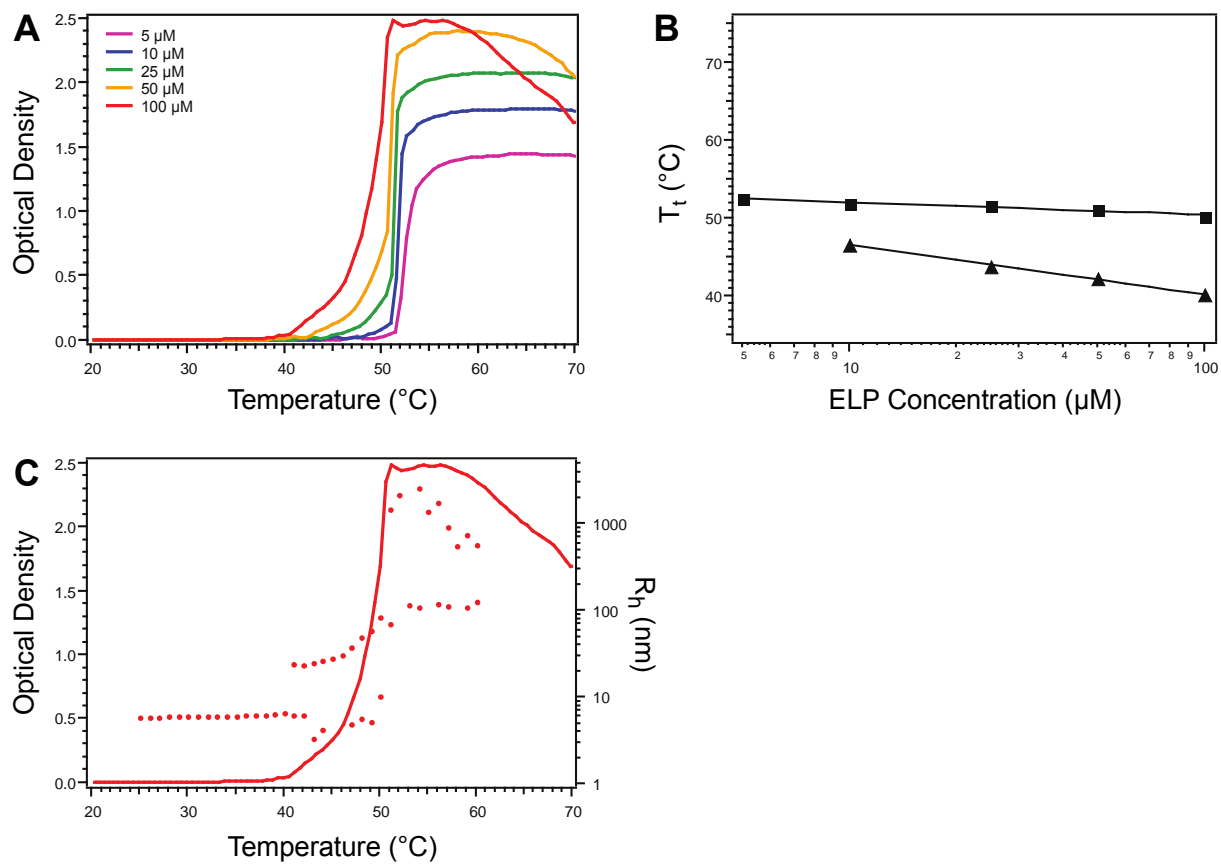


**Figure S22.** Thermal characterization of ELP-V-SVB<sub>1</sub>-S by temperature-regulated turbidimetry and DLS. A) ELP-V-SVB<sub>1</sub>-S was characterized by temperature-regulated turbidimetry in PBS at ELP concentrations of 5, 10, 25, 50, and 100 μM. B) The T<sub>t</sub>s at each concentration were

determined as the temperatures corresponding to the maximum of the Gaussian fit of the derivative of OD with respect to temperature (squares), which were fit to a logarithmic relationship (line). The CMTs at each concentration were approximated as the temperatures corresponding to the positive divergences of OD from baseline (triangles), which were fit to a logarithmic relationship (line). Turbidimetry was not sensitive enough to determine the CMT below 10  $\mu\text{M}$ . C) DLS measurement of  $R_h$  (dots, right ordinate) at 100  $\mu\text{M}$  corroborated the self-assembly with respect to temperature as determined by turbidimetry (line, left ordinate).

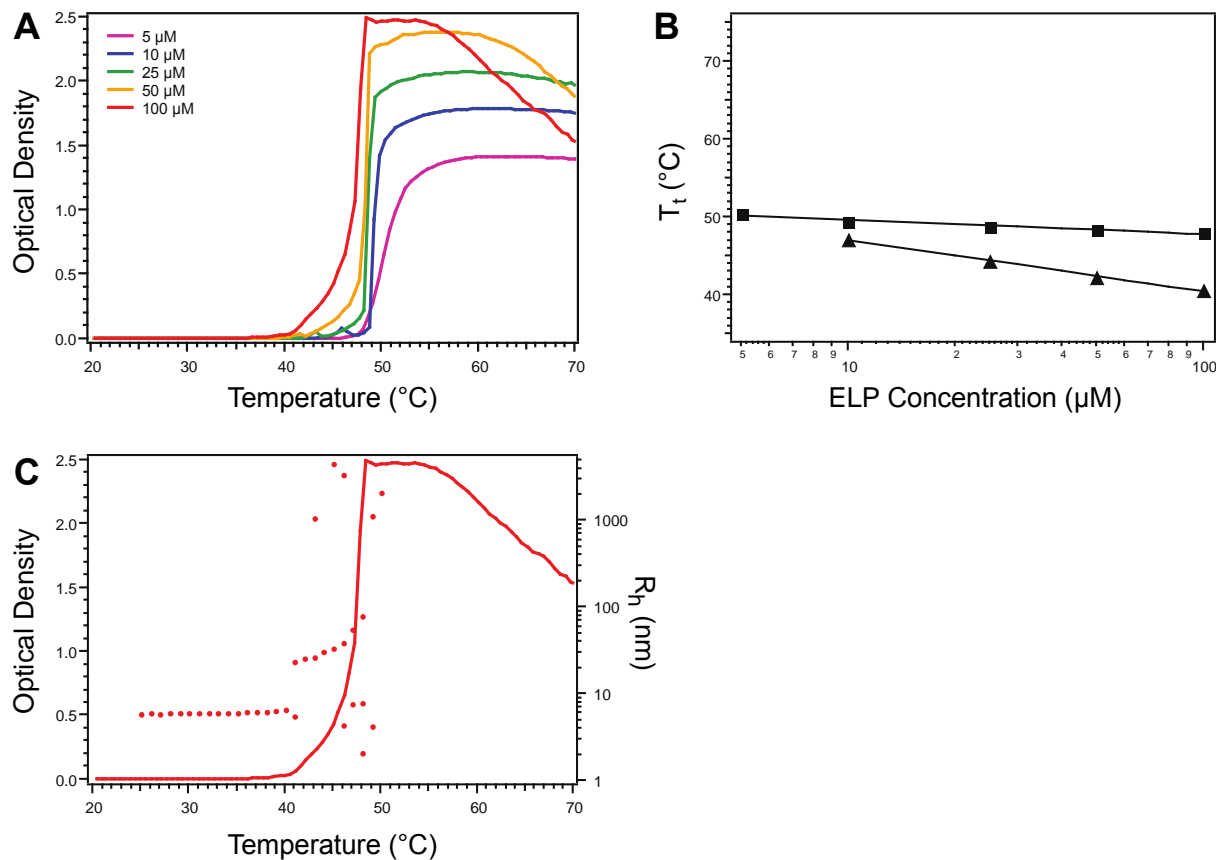


**Figure S23.** Thermal characterization of ELP-V-SVB<sub>5</sub>-S by temperature-regulated turbidimetry and DLS. A) ELP-V-SVB<sub>5</sub>-S was characterized by temperature-regulated turbidimetry in PBS at ELP concentrations of 5, 10, 25, 50, and 100  $\mu\text{M}$ . B) The  $T_f$ s at each concentration were determined as the temperatures corresponding to the maximum of the Gaussian fit of the derivative of OD with respect to temperature (squares), which were fit to a logarithmic relationship (line). The CMTs at each concentration were approximated as the temperatures corresponding to the positive divergences of OD from baseline (triangles), which were fit to a logarithmic relationship (line). Turbidimetry was not sensitive enough to determine the CMT below 10  $\mu\text{M}$ . C) DLS measurement of  $R_h$  (dots, right ordinate) at 100  $\mu\text{M}$  corroborated the self-assembly with respect to temperature as determined by turbidimetry (line, left ordinate).

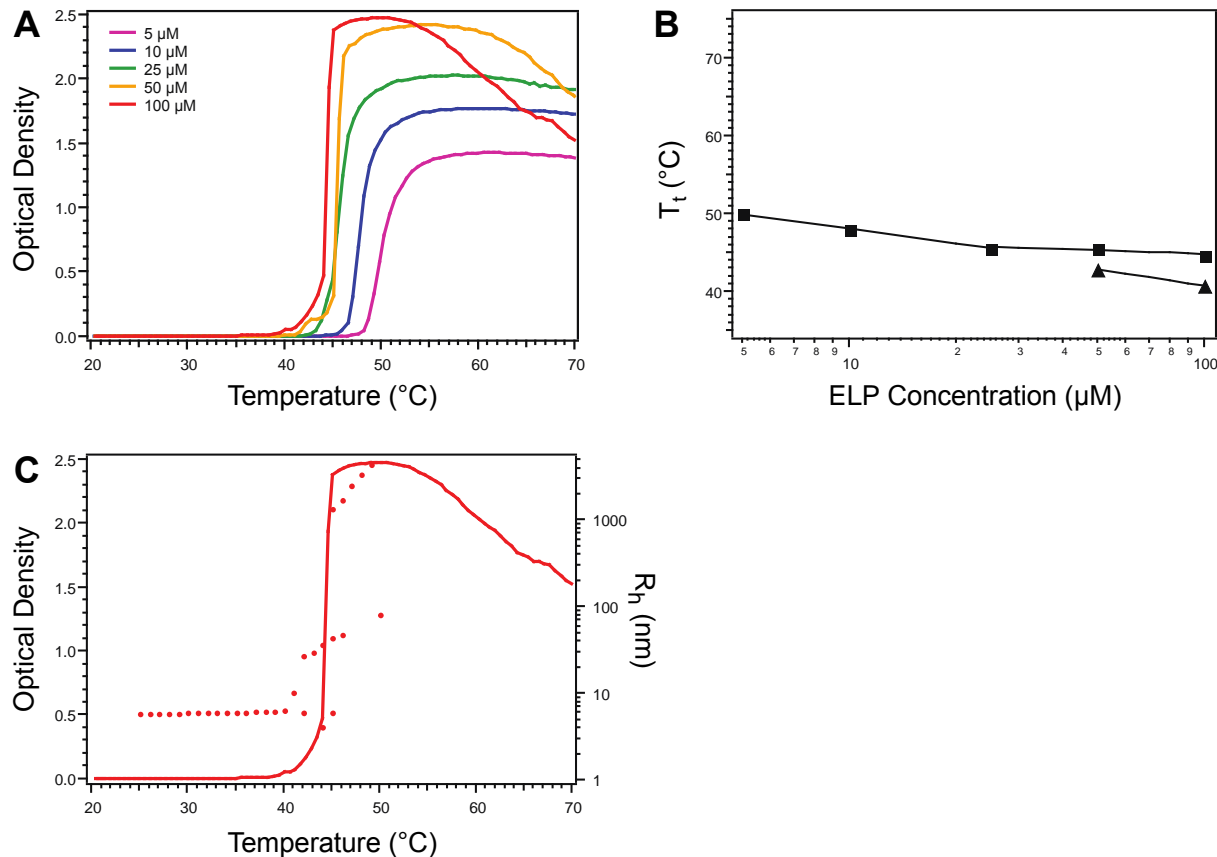


**Figure S24.** Thermal characterization of ELP-V-SVB<sub>10</sub>-S by temperature-regulated turbidimetry and DLS. A) ELP-V-SVB<sub>10</sub>-S was characterized by temperature-regulated turbidimetry in PBS at ELP concentrations of 5, 10, 25, 50, and 100  $\mu\text{M}$ . B) The  $T_{\text{ts}}$  at each concentration were determined as the temperatures corresponding to the maximum of the Gaussian fit of the derivative of OD with respect to temperature (squares), which were fit to two separate logarithmic relationships for 5-25  $\mu\text{M}$  and 25-100  $\mu\text{M}$  (line). The CMTs at each concentration were approximated as the temperatures corresponding to the positive divergences of OD from baseline (triangles), which were fit to a logarithmic relationship (line). No CMT was evident below 50  $\mu\text{M}$  by turbidimetry, which was supported by the difference in slope of the logarithmic fit to the measured  $T_{\text{ts}}$  above and below 50  $\mu\text{M}$ . C) DLS measurement of  $R_h$  (dots, right ordinate) at 100  $\mu\text{M}$  corroborated the self-assembly with respect to temperature as determined by turbidimetry (line, left ordinate).

**Table S11.**  $T_{\text{ts}}$  of blocky interface ELPs.<sup>1</sup>

ELP	ELP concentration ( $\mu\text{M}$ )				
	5	10	25	50	100
V-SVB <sub>1</sub> -S	52.48	51.83	51.52	51.16	50.12
V-SVB <sub>5</sub> -S	50.35	49.32	48.71	48.35	47.85
<b>V-SVB<sub>10</sub>-S</b>	<b>49.97</b>	<b>47.92</b>	<b>45.56</b>	<b>45.60</b>	<b>44.62</b>

<sup>1</sup> $T_{\text{ts}}$  were calculated as the temperature corresponding to the maximum of the Gaussian fit of the derivative of OD, with respect to temperature, reported in  $^{\circ}\text{C}$ . This  $T_t$  corresponded to the

aggregation of ELP into micron-scale coacervates, indicative of the nanoparticle-to-aggregate transition.

**Table S12.** CMTs of blocky interface ELPs.<sup>1</sup>

ELP	ELP concentration ( $\mu\text{M}$ )			
	10	25	50	100
<b>V-SVB<sub>1</sub>-S</b>	46.52	43.77	42.17	40.07
<b>V-SVB<sub>5</sub>-S</b>	47.07	44.32	42.17	40.57
<b>V-SVB<sub>10</sub>-S</b>	NM <sup>2</sup>	NM <sup>2</sup>	42.77	40.67

<sup>1</sup>The CMT, corresponding to the temperature at which the unimer-to-nanoparticle transition occurred, was approximated as the temperature at which the OD deviated positively from baseline, reported in °C. Due to the limited sensitivity of turbidimetry to self-assembled nanoparticles at low concentrations, approximations were not made at 5  $\mu\text{M}$ .

<sup>2</sup>No CMT was evident for measurement of ELP-V-SVB<sub>10</sub>-S at concentrations of 25  $\mu\text{M}$  and lower.

**Table S13.** Fit parameters of blocky interface ELP  $T_{ts}$ .<sup>1</sup>

ELP	<i>m</i> (°C)	<i>b</i> (°C)	<i>r</i> <sup>2</sup>
<b>V-SVB<sub>1</sub>-S</b>	-0.70	53.61	0.930
<b>V-SVB<sub>5</sub>-S</b>	-0.79	51.38	0.961
<b>V-SVB<sub>10</sub>-S</b>	-2.74 <sup>2</sup>	54.32 <sup>2</sup>	0.999 <sup>2</sup>
	-0.68 <sup>3</sup>	47.90 <sup>3</sup>	0.715 <sup>3</sup>

<sup>1</sup>Parameters according to Equation S2, fit to  $T_{ts}$  measured at 5-100  $\mu\text{M}$ .

<sup>2</sup>Fit to  $T_{ts}$  at concentrations 5-25  $\mu\text{M}$ .

<sup>3</sup>Fit to  $T_{ts}$  at concentrations 25-100  $\mu\text{M}$ .

**Table S14.** Fit parameters of blocky interface ELP CMTs.<sup>1</sup>

ELP	<i>m</i> (°C)	<i>b</i> (°C)	<i>r</i> <sup>2</sup>
<b>V-SVB<sub>1</sub>-S</b>	-2.76	52.82	0.998
<b>V-SVB<sub>5</sub>-S</b>	-2.86	53.56	0.997
<b>V-SVB<sub>10</sub>-S</b>	-3.03 <sup>2</sup>	54.62 <sup>2</sup>	1.000 <sup>2</sup>

<sup>1</sup>Parameters according to Equation S2, fit to CMTs approximated at 10-100  $\mu\text{M}$ .

<sup>2</sup>Fit to CMTs approximated at 50-100  $\mu\text{M}$ .

**Table S15.** Refractive index increment of blocky interface ELPs.

ELP	dn/dc (mL/mg)	<i>r</i> <sup>2</sup>
<b>V-SVB<sub>1</sub>-S</b>	$1.703658 \times 10^4$	0.999
<b>V-SVB<sub>5</sub>-S</b>	$1.718044 \times 10^4$	0.999
<b>V-SVB<sub>10</sub>-S</b>	$1.692355 \times 10^4$	0.999

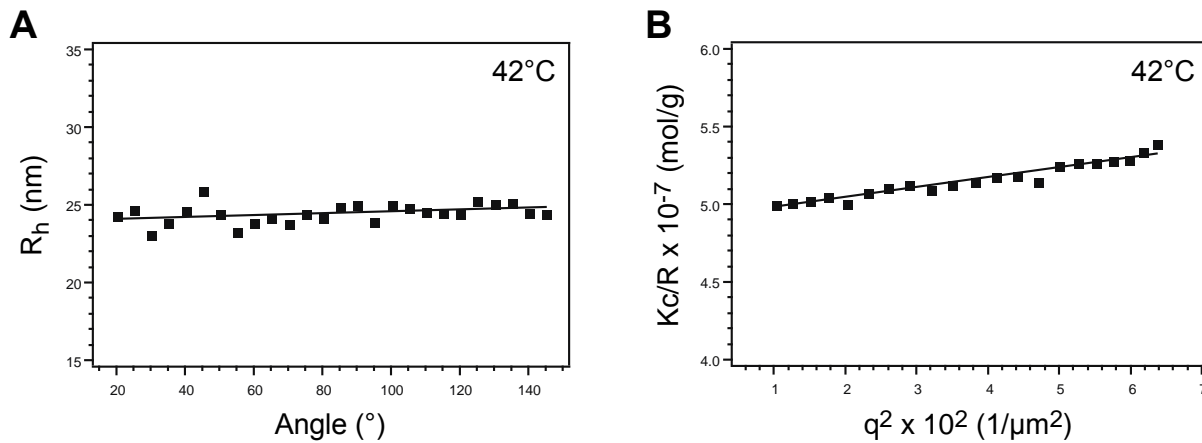


**Figure S25.** DLS and SLS characterization of ELP-V-SVB<sub>1</sub>-S. A) R<sub>h</sub> was determined from DLS measurements and B) R<sub>g</sub> and MW was determined from SLS measurements of 100  $\mu\text{M}$  solution at 42°C, 2°C above the CMT of ELP-V-SVB<sub>1</sub>-S. Markers represent individual measurements while solid lines represent linear fits to the data.

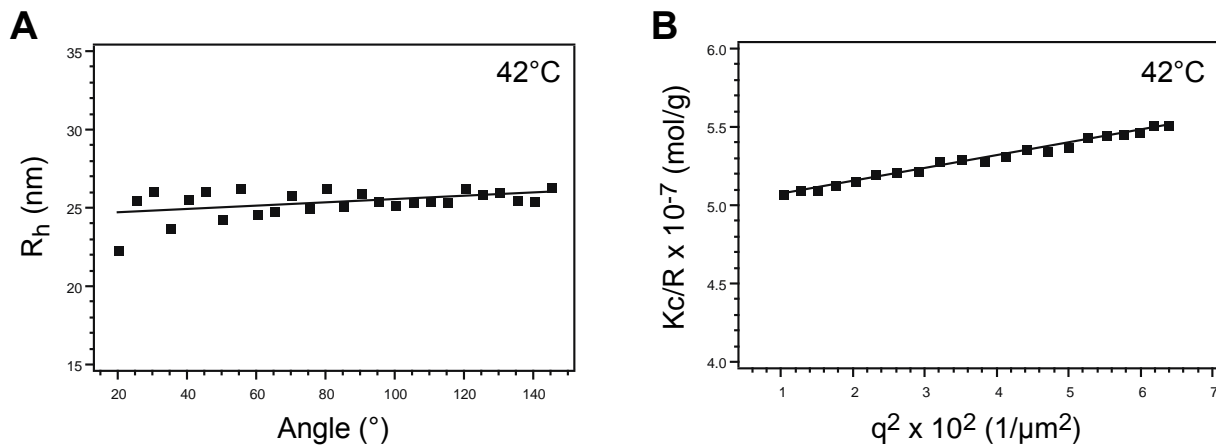


**Figure S26.** DLS and SLS characterization of ELP-V-SVB<sub>5</sub>-S. A) R<sub>h</sub> was determined from DLS measurements and B) R<sub>g</sub> and MW was determined from SLS measurements of 100  $\mu\text{M}$  solution at 42°C, 2°C above the CMT of ELP-V-SVB<sub>5</sub>-S. Markers represent individual measurements while solid lines represent linear fits to the data.

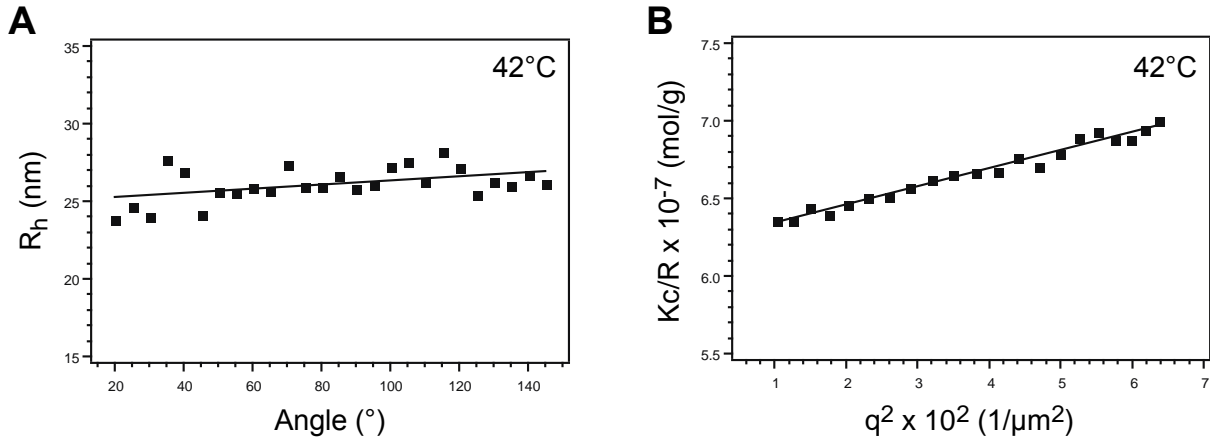


**Figure S27.** DLS and SLS characterization of ELP-V-SVB<sub>10</sub>-S. A) R<sub>h</sub> was determined from DLS measurements and B) R<sub>g</sub> and MW was determined from SLS measurements of 100 μM solution at 42°C, 2°C above the CMT of ELP-V-SVB<sub>10</sub>-S. Markers represent individual measurements while solid lines represent linear fits to the data.

**Table S16.** Summary of SLS and DLS characterization of blocky interface ELP self-assembly at 42°C.

ELP	R <sub>g</sub> (nm)	R <sub>h</sub> (nm)	ρ (R <sub>g</sub> /R <sub>h</sub> )	MW (g/mol)	N <sub>agg</sub>
<b>V-SVB<sub>1</sub>-S</b>	19.9 (±2.9%)	24.0	0.83	2.033 x 10 <sup>6</sup> (±0.31%)	42
<b>V-SVB<sub>5</sub>-S</b>	22.1 (±1.3%)	24.5	0.90	2.001 x 10 <sup>6</sup> (±0.17%)	41
<b>V-SVB<sub>10</sub>-S</b>	23.7 (±1.8%)	25.0	0.95	1.605 x 10 <sup>6</sup> (±0.28%)	33

**Table S17.** Molecular volume, scattering length, and scattering length density values for block copolypeptides and H<sub>2</sub>O.

ELP	Molecular volume (nm <sup>3</sup> )	Scattering length (nm)	Scattering length density (nm <sup>-2</sup> )
<b>SVT<sub>svs</sub></b>	62.9	7.31 x 10 <sup>-2</sup>	1.16 x 10 <sup>-3</sup>
<b>SVD<sub>sv</sub></b>	62.9	7.31 x 10 <sup>-2</sup>	1.16 x 10 <sup>-3</sup>
<b>H<sub>2</sub>O</b>	3.0 x 10 <sup>-2</sup>	2.82 x 10 <sup>-5</sup>	9.40 x 10 <sup>-4</sup>

The form factor for a core-shell spherical micelle was developed by Gerstenberg and Pedersen,<sup>5</sup> and consists of four contributions: the self-correlation of the micelle core, the self-correlation of the chains that form the corona, cross-correlation between the core and chains, and cross-correlation between different chains.

$$P(q) = N_{agg}^2 \beta_s^2 P_s(q) + N_{agg} \beta_c^2 P_c(q) + 2N_{agg}^2 \beta_s \beta_c S_{sc}(q) + N_{agg}(N_{agg} - 1) \beta_c^2 S_{cc}(q) \quad (S4)$$

where N<sub>agg</sub> is the aggregation number of the micelle, β<sub>s</sub> and β<sub>c</sub> are the scattering lengths of the spherical core and corona chains, respectively. P<sub>s</sub> and P<sub>c</sub> are the form factors of the spherical core

and corona chains,  $S_{sc}$  is the cross-correlation between the spherical core and chains, and  $S_{cc}$  is the cross-correlation between the chains.

The form factor of the spherical core is given by:

$$P_s(q) = \Phi^2(qR) \quad (\text{S5})$$

where

$$\Phi(qR) = \frac{3[\sin(qR) - qR\cos(qR)]}{(qR)^3}. \quad (\text{S6})$$

Corona chains with radius  $R_g$  have a self-correlation term as follows:

$$P_c(q) = \frac{2[\exp(-x) - 1 + x]}{x^2} \quad (\text{S7})$$

which =  $q^2 R_g^2$ .

Gerstenberg and Pedersen mimicked non-penetration of the corona chains into the core by modeling them to start at distance  $R_g$  from the surface of the core. Thus:

$$S_{sc}(q) = \Phi(qR)\varphi(qR_g) \frac{\sin(q[R+dR_g])}{q[R+dR_g]}. \quad (\text{S8})$$

The function  $\varphi(x) = [1 - \exp(-x)] / x$  is the form factor of a Gaussian polymer chain. The interaction term between the chains is:

$$S_{cc}(q) = \varphi^2(qR_g) \left[ \frac{\sin(q[R+dR_g])}{q[R+dR_g]} \right]^2. \quad (\text{S9})$$

## References

- (1) McDaniel, J. R.; Mackay, J. A.; Quiroz, F. G.; Chilkoti, A., Recursive directional ligation by plasmid reconstruction allows rapid and seamless cloning of oligomeric genes. *Biomacromolecules* **2010**, *11* (4), 944-52.
- (2) Meyer, D. E.; Chilkoti, A., Genetically encoded synthesis of protein-based polymers with precisely specified molecular weight and sequence by recursive directional ligation: examples from the elastin-like polypeptide system. *Biomacromolecules* **2002**, *3* (2), 357-67.
- (3) Cho, Y.; Zhang, Y.; Christensen, T.; Sagle, L. B.; Chilkoti, A.; Cremer, P. S., Effects of Hofmeister anions on the phase transition temperature of elastin-like polypeptides. *The journal of physical chemistry. B* **2008**, *112* (44), 13765-71.
- (4) Meyer, D. E.; Chilkoti, A., Quantification of the effects of chain length and concentration on the thermal behavior of elastin-like polypeptides. *Biomacromolecules* **2004**, *5* (3), 846-51.
- (5) Pedersen, J. S.; Gerstenberg, M. C., Scattering Form Factor of Block Copolymer Micelles. *Macromolecules* **1996**, *29* (4), 1363-1365.